# Finite Element Analysis of Temperature Distribution during Arc Welding Using Adaptive Grid Technique

*A transient adaptive mesh is developed that makes it possible to determine temperature distribution at the arc with less computational time*

BY N. SILVA PRASAD AND T. K. SANKARA NARAYANAN

ABSTRACT. Analysis of temperature and the cooling rates during the welding process is essential to determine the deformation and residual stresses, and hence, the load-carrying capacity of the weldments. Numerical methods with nonlinear temperature-dependent mechanical properties with latent heat effects have been developed in recent years. The accuracy and computational efficiency of these methods depend on the input mesh used in the analysis. In this paper, a transient adaptive mesh, which gives a fine mesh around the arc source where temperature gradients are too high and a coarse mesh in other places, is developed. The computed values of temperature for a sample problem are compared with the experimental results available in the literature. The mesh and temperature plots at different times are presented.

## Introduction

Rosenthal (Ref. 1) was the first to develop a closed form solution to the temperature distribution of weldments by considering a moving heat source. The accuracy of this method is reasonably good in dealing with temperature calculations in the areas not too close to the welding arc, but it is poor in the weld metal and heat-affected zone. The accuracy in estimation of temperatures in these regions is very important since they are critical areas where high tensile residual stress results. Various researchers developed numerical methods to predict better temperature distribution. Comini, *et al.* (Ref. 2), developed a finite element method to address the nonlinear unsteady heat conduction problem involving temperature-dependent thermophysical properties. Morgan, *et al.* (Ref. 3), developed an enthalpy method, which includes latent heat effects in predicting temperatures of two-dimensional bodies involving phase change. The effect of heat source shape in temperature calculations is considered in Refs. 4–6. John Goldak (Ref. 7) suggests that the thrust area in welding is adaptive and dynamic meshing.

The accuracy of the finite element method depends upon the mesh that is used in the analysis. The temperature around the arc is higher than the melting point of the material, and it drops sharply in the regions just away from the arc. This requires an extremely fine mesh in the confined high-temperature region to predict the temperature accurately in that region. But the computational time increases with the fineness of mesh. Since fine mesh is required only around the arc source, adaptivity of the input mesh according to the position of the arc source is efficient. The adaptive grid technique gives a fine mesh in the high-temperature region around the arc and a coarse mesh in other regions at any time step. With this it is possible to achieve desired accuracy with less computation time.

In this paper we have implemented an adaptivity technique in the weld temperature calculations. The temperature-dependent mechanical properties are considered by predictor corrector iterative method. Latent heats are taken as nodal force vector, and the heat source is assumed to be a Gaussian one.

**KEY WORDS**

FEM
Temperature Distribution
Arc Welding
Adaptive Mesh
Delaunay Triangulation
Nonlinear
Geometry Discretization
Error Estimation
Mesh Refinement
Structured Mesh

### Temperature Analysis

The governing equation for the temperature analysis is taken as

$$\rho c_{i-1}\frac{\partial T_i}{\partial t} = \frac{\partial}{\partial x}\left[k_{i-1}\frac{\partial T_i}{\partial x}\right] + \frac{\partial}{\partial y}\left[k_{i-1}\frac{\partial T_i}{\partial y}\right] \quad (1)$$

With boundary condition as

$$k_{i-1}\frac{\partial T_i}{\partial n} + h(T_i - T_\infty) = 0.0 \quad t > 0 \quad (2)$$

and

$$T = T_\infty \quad \text{for } t = 0 \quad (3)$$

In the above equation, i denotes the iteration number. Since radiation losses are small, they are neglected in this analysis. Temperature dependency of the convective coefficient is also neglected in this analysis. The thermal conductivity and specific heat relationships with temperature are taken as in Fig. 1 (Ref. 8).

*N. SILVA PRASAD and T. K. SANKARA NARAYANAN are with the Department of Mechanical Engineering, Indian Institute of Technology, Madras, India.*

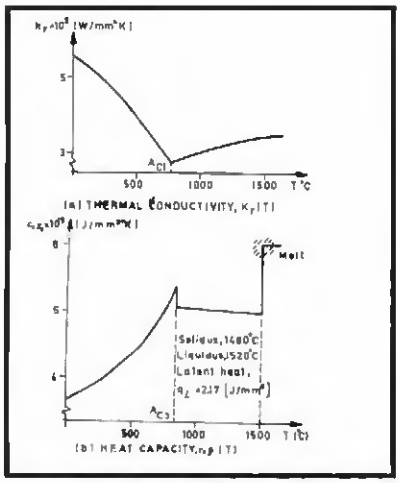


*Fig. 1 — Thermal properties of mild steel St 37. A — Thermal conductivity, Kt (T); B — heat capacity, Cvp (T).*

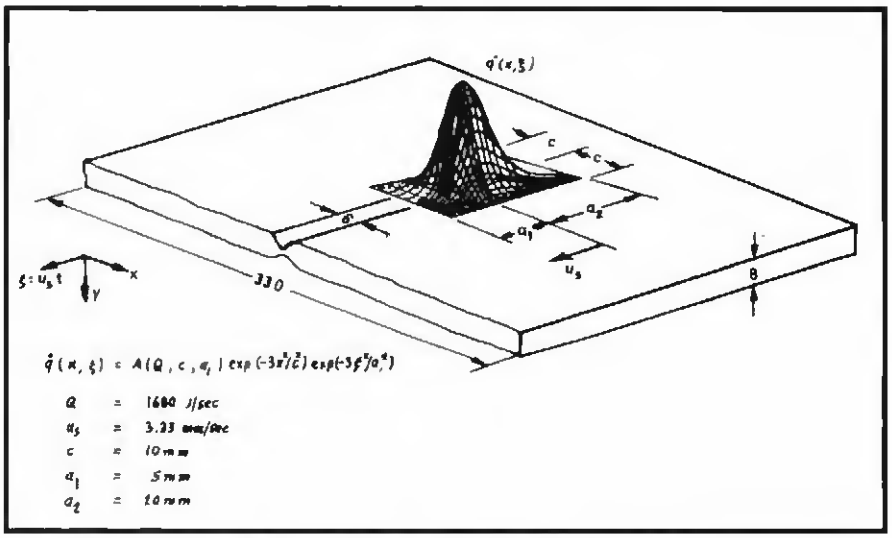


*Fig. 2 — Gaussian power-density distribution of heat input from moving arc.*

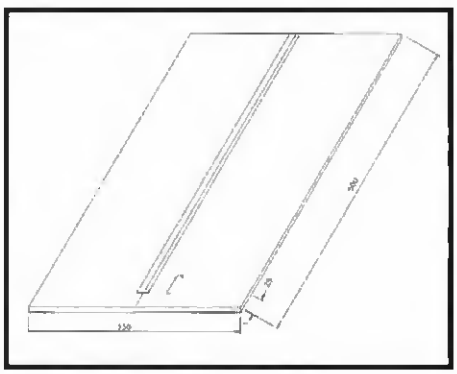


*Fig. 3 — Arc welding of a steel plate.*

The thermal conductivity and specific heat capacity shown in these figures are converted into polynomial equations using grapher package. Care is taken to take the sample points at closer intervals in order to maintain the accurate interpolation at any intermediate temperature.

The latent heat effects are considered in the analysis as in Ref. 9. The latent heat evolved for the elements undergoing phase transition in the previous time step was incorporated as a nodal force vector. The heat source is assumed as Gaussian distribution as shown in Fig. 2 (Ref. 8).

The weak formulation of Equation 1 is given as

$$\int_\Omega \rho c\, T_{,t}\, \overline{T}\, d\Omega + \int_\Omega K_{ij} T_{,j}\, \overline{T}_{,i}\, d\Omega + \int_\tau h(T - T_a)\overline{T}\, d\tau - \int_\Omega q\, \overline{T}\, d\Omega = 0 \quad (4)$$

Having obtained the weak form of the differential equation, suitable shape functions are assumed for the temperature T. The general finite element equilibrium equation can be expressed as

$$[M]\{\dot{T}\} + [K]\{T\} = \{f\} \quad (5)$$

**Time Dependent Solution**

The fully implicit backward algorithm with predictor corrector technique for temperature-dependent mechanical properties is used to solve the Equation 5. This reduces the ordinary differential equation to the following algebraic system of equations.

$$\{[M] + \Delta t[K]\}\{T\}_{n+1} = [M]\{T\}_n + \Delta t\{F\}_n \quad (6)$$

where n = 1, 2, ... N denotes the time step level.

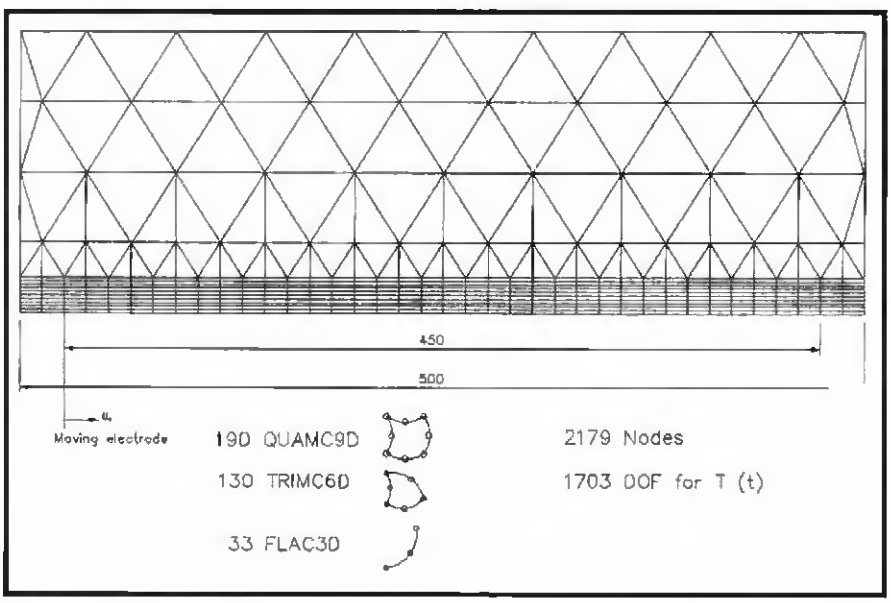


*Fig. 4 — Mesh used in Ref. 8.*

**Table 1 — Comparison of NDOF**

| | NDOF for Adaptive Mesh Case 1 | NDOF for Adaptive Mesh Case 2 | NDOF for Structured Mesh (Fig. 4) |
|---|---|---|---|
| Start of welding (7.5 s) | 269 | 331 | 1703 |
| Middle of welding (37.5 s for Case 1) (75 s for Case 2) | 330 | 431 | 1703 |
| End of welding | 235 | 348 | 1703 |

### Mesh Generation and Adaptivity

In the present work, adaptive mesh algorithms based on Joe and Simpson (Ref. 10) and Delaunay triangulation (Ref. 11) are used, as they have the advantage of generating nearly equilateral triangular meshes. The steps involved in the adaptive grid technique are as follows:

1) Discretizing the given geometry of weldment.

2) Temperature calculation for the initial mesh.

3) Estimating the discretization error.

4) Refining the mesh by adaptivity.

5) Go to Step 2 for next time step.

### Discretization of Given Geometry

The given geometry is first subdivided into complex subdomains to avoid the spillover of triangles outside the boundaries in the multiply connected regions and concave domains. This takes care of meshing the welding plates with holes or cuts in it. Each convex subdomain is then triangulated using the Delaunay triangulation method. The Delaunay triangulation of a set of nodes produces a convex hull, defined as the smallest convex re-

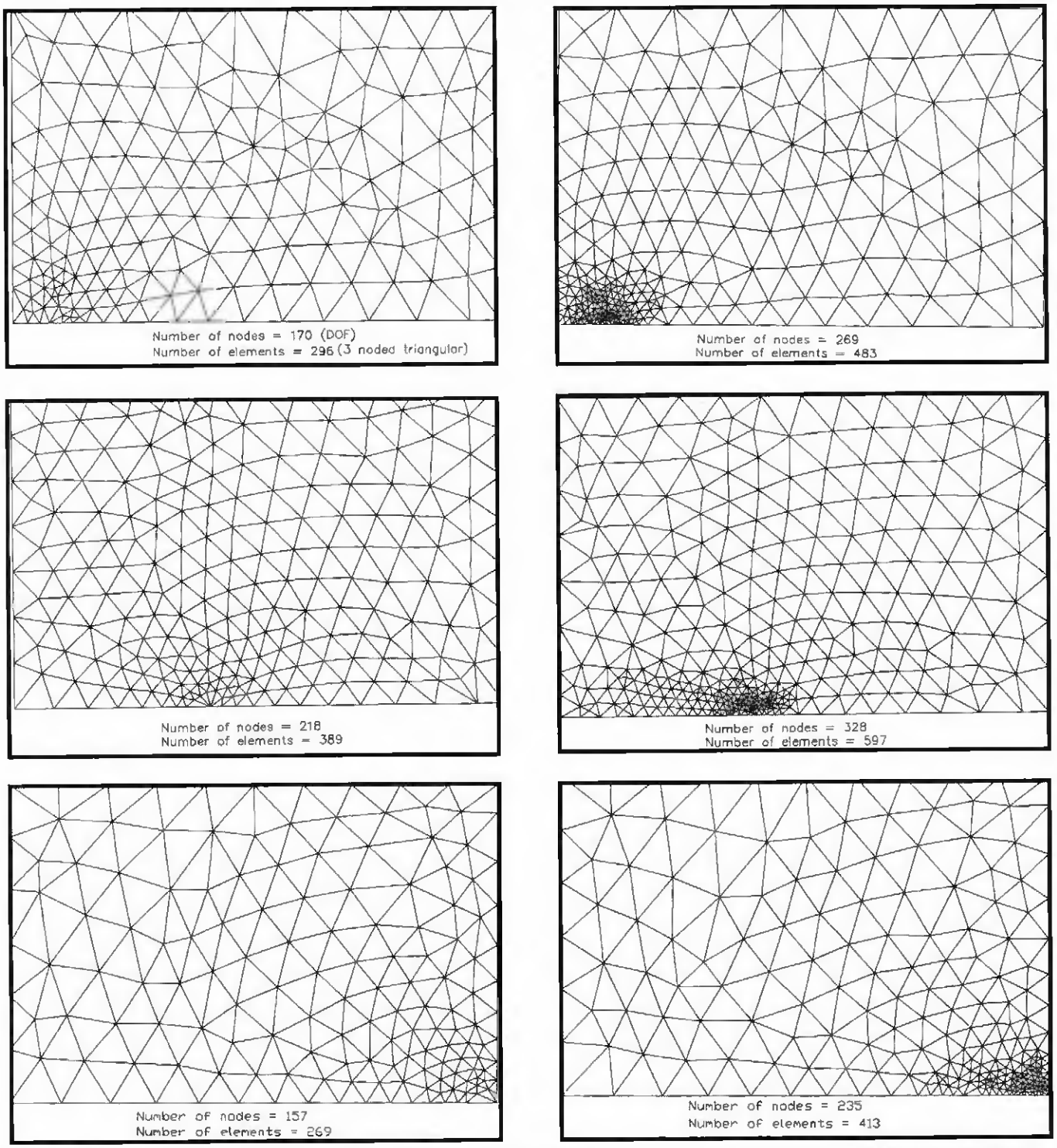


*Fig. 5 — Mesh for 250-mm plate. A — Initial mesh at 7.5 s; B — adaptive mesh at 7.5 s; C — initial mesh at 30 s; D — adaptive mesh at 30 s; E — initial mesh at 75 s; F — adaptive mesh at 75 s.*

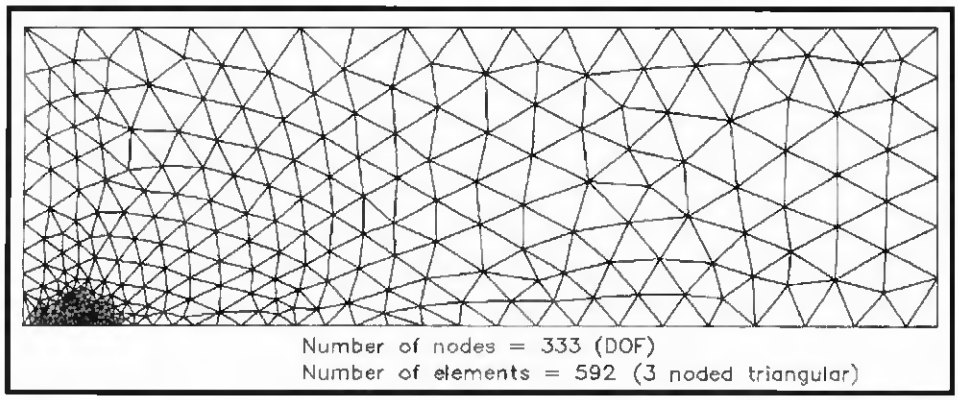


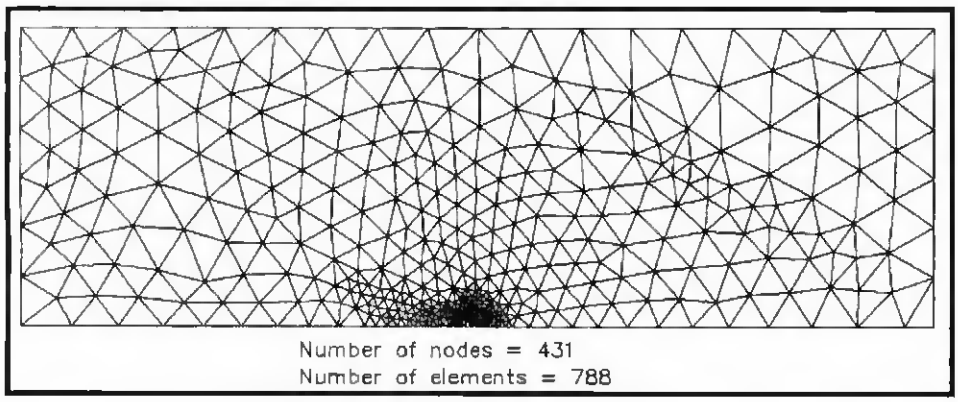


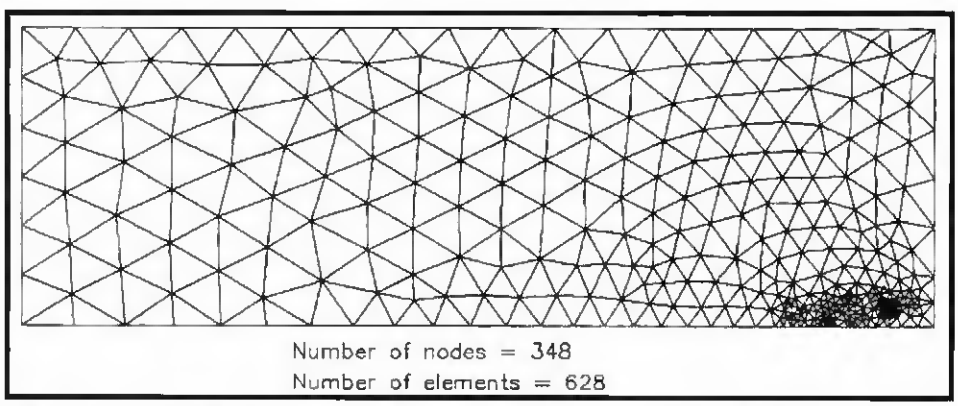


*Fig. 6 — Mesh for 500-mm plate. A — Adaptive mesh at 7.5 s; B — adaptive mesh at 75 s; C — adaptive mesh at 150 s.*

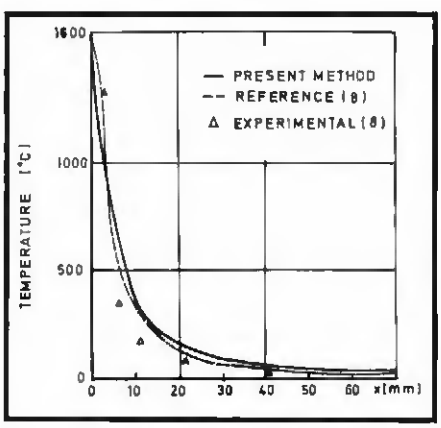


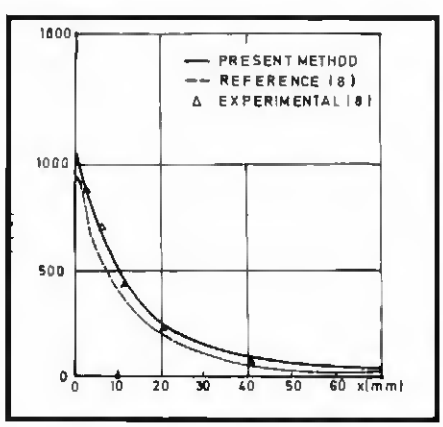


*Fig. 7 — Transverse temperature distribution. A — At midsection during passing arc; B — at midsection 7.5 s after passing arc.*

gion enclosing all the points in the domain. Hence, the boundary triangulation of a convex subdomain produces a convex hull which is identical to the boundary of the polygon.

Discretization of each initial triangulated subdomain includes distribution of well-placed nodes on the boundaries and interior of the domain and triangulation of these nodes. Initially, each node is assigned a spacing value. A node spacing function of each element is then defined as a linear interpolation of the nodal spacing values of its vertices. Nodal spacing functions are then used to place additional nodes on the boundaries and interior of the elements. The node that corresponds to the arc position is given a lesser spacing value compared to the other boundary nodes. This gives an input mesh which is slightly finer in the arc source region as shown in Fig. 5A, C, and E. This makes the adaptive analysis to converge within one or two iterations. Care has been taken to avoid the placement of nodes outside the domain. Then nodes are remeshed by Delaunay triangulation. The nodal spacing is adaptively computed in the course of analysis. However, to initiate the process, at certain initial nodes, the nodal spacing function needs to be given as additional input. In the present case, therefore, the nodal spacing function at the four corners of the rectangular domain analyzed as also at the node corresponding to the initial arc position is given as input.

The initial mesh, which includes some odd-shaped triangles, is then smoothed using Laplacian smoothing techniques. This gives a smooth graded mesh with triangles of improved shape. In this technique, each node inside the geometry is moved successively to the centroid of its neighbors and several iterations are made through the entire set of interior nodes. Care has been taken to avoid the nodes to be moved outside the boundary.

### Error Estimation and Adaptivity

A simple error indicator for h-refinement as in Ref. 12 is applied to give an indication of the accuracy of the computed solution. The temperature field obtained from the finite element analysis is T, and $\tilde{T}$ is the projected value obtained through the interpolation of nodal values. The error is then defined in terms of temperature gradients $\partial T/\partial x$, $\partial T/\partial y$, etc.

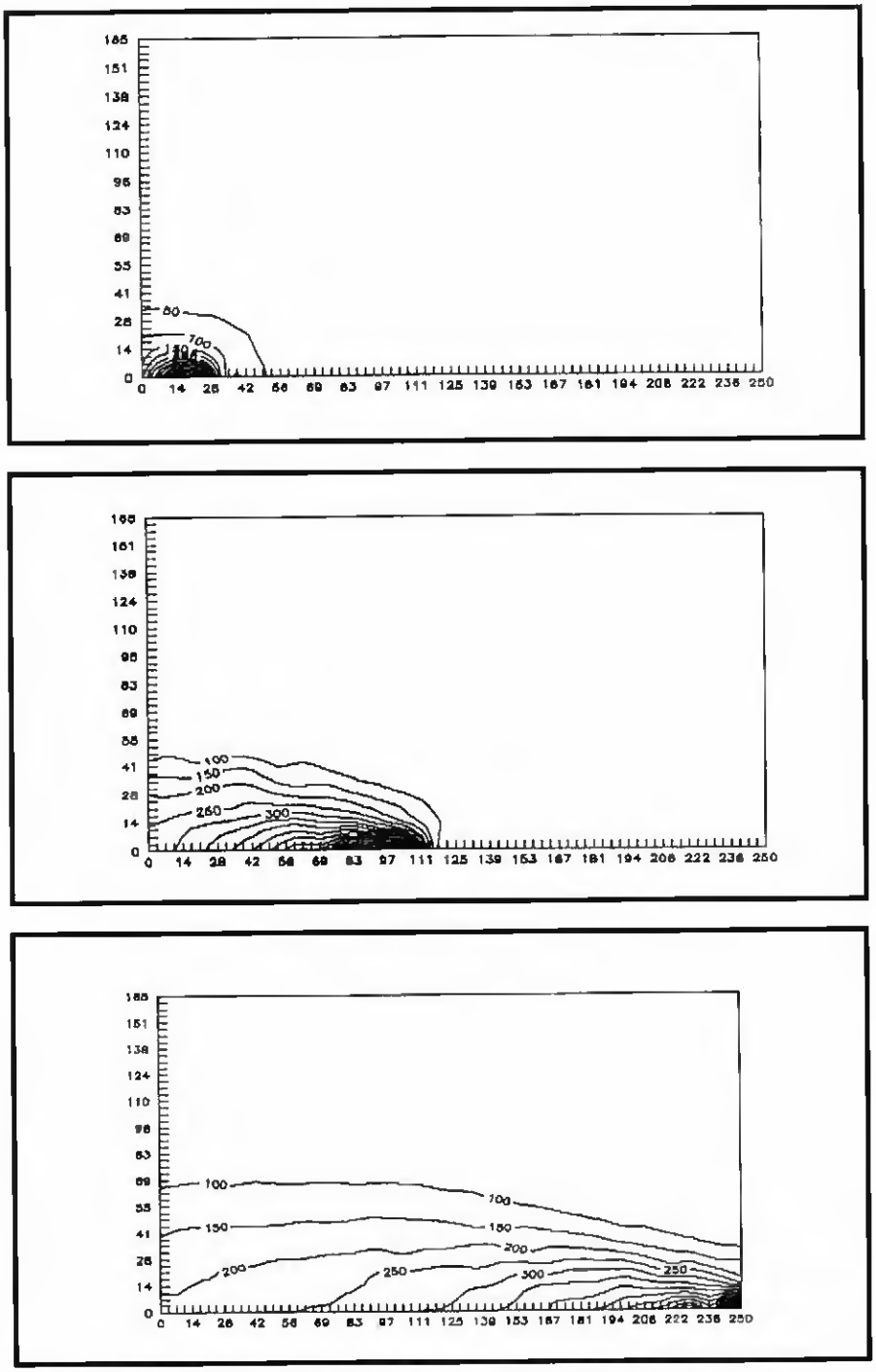


*Fig. 8 — Temperature plot (°C) for 250-mm-long (x-axis) and 165-mm-wide (y-axis) plate. A — Temperature plot at 5 s; B — temperature plot at 30 s.*

Since heat flux q is based on temperature gradients, error can be defined as

$$e = \bar{q} - q \tag{7}$$

The error in each element is calculated according to the equation

$$\|e\|_e = \left\{ k \int_\Omega \left\{ \left( \frac{\partial \bar{T}}{\partial x} - \frac{\partial T}{\partial x} \right)^2 + \left( \frac{\partial \bar{T}}{\partial y} - \frac{\partial T}{\partial y} \right)^2 \right\} dxdy \right\}^{1/2} \tag{8}$$

Similar to energy norm in the stress analysis, here a quantity ||q|| considered to be a measure of total heat dissipation in the whole domain is given by the equation

$$\|q\|^2 = \sum_{i=1} k \int_\Omega \left\{ \left( \frac{\partial T}{\partial x} \right)^2 + \left( \frac{\partial T}{\partial y} \right)^2 \right\} dxdy \tag{9}$$

where n is the total number of elements in the mesh.

For an optimum analysis, the error in each element must be approximately equal. Hence, the maximum allowable error in each element is calculated using the relation

$$\|\bar{e}\|_e \le \bar{\eta} \left( \frac{\|q\|^2}{n} \right)^{1/2} \tag{10}$$

where $\bar{\eta}$ is the maximum error specified by the user.

The error computed for each element $\|e\|_e$ is compared with that of the maximum allowable error $\|\bar{e}\|_e$ and is given by the ratio

$$\xi_e = \frac{\|e\|_e}{\|\bar{e}\|_e} \tag{11}$$

If $\xi_e$ for an element is greater than 1, then the size of the element must be reduced, and if it is less than 1, the size is to be enlarged. The element sizes are reduced by decreasing the nodal spacing values of these elements. At the vertices of these elements,

$$New\ SF_{e,j} = min \left( old\ SF_{e,i} / \xi_{ek} \right)^{1/\sqrt{n}} \tag{12}$$

where j refers to a vertex of the element, e, and k refer to the neighbors of the element e, which have j as a common vertex.

According to the new nodal spacing values, additional nodes are placed and entire nodes are remeshed. The mesh is then smoothed. Finite element analysis is carried out for the new mesh. This process is repeated until the error is within the prescribed level. Then analysis is carried out for next time step.

### Example Problem

To verify the validity and the advantages of the above formulations, a problem given in Ref. 8 is considered. The welding conditions are taken as mentioned in Fig. 2. The dimensions of the welding plate are taken as shown in Fig. 3. The grid used in Ref. 8 for the temperature analysis is shown in Fig. 4. In the present analysis, two cases of different weld lengths are considered. The other parameters remain the same for both cases.

Case 1: weld length of 250 mm (9.8 in.).

Case 2: weld length of 500 mm (19.7 in.).

The other inputs given to the computer are as follows:

1) Total heat input of 1680 W.

2) Initial condition (room temperature) = 30°C (86°F).

3) Weld speed of 3.33 mm/s (7.86

in./min).

4) Permissible error norm is 0.1.

5) Nodal spacing value for nodes at the four corners of the plate = 5.

6) Nodal spacing value for the node at the initial arc position = 20.

## Results and Discussion

The initial and adapted meshes at different times for a 250-mm-length plate are shown in Fig. 5A–F. The meshes for 500-mm plate are shown in Fig. 6A–C. The number of degrees of freedom (NDOF) for the different meshes used in the analysis are compared in Table 1.

The temperature distributions at the midsection for Case 2 are plotted in Fig. 7A and B for the instant when the arc passes this section and 7.5 s thereafter. The computed values show good agreement with the experimental results used in Ref. 8. The temperature isotherms for Case 1 are shown in Fig. 8A–C.

## Conclusion

From the above discussions, it can be inferred that by the adaptive mesh generation technique it is possible to compute the temperature distribution of welded plate with reduced NDOF. In the subsequent elasto-plastic residual stress analysis for full plate, several iterations are to be made. Hence, reduction in the number of nodes will reduce the computational time substantially.

## Nomenclature

| | |
|---|---|
| $k$ | Thermal conductivity in w/m°C |
| $\rho$ | Mass density in kg/m$^3$ |
| $c$ | Specific heat in J/kg°C |
| $h$ | Convective heat transfer coefficient in w/m$^2$°C |
| $T_\infty$ | Ambient temperature |
| $[M]$ | Heat capacity matrix |
| $[K]$ | Conductivity matrix |
| $\{f\}$ | Nodal force vector |

*References*


1. Rosenthal, D. 1941. Mathematical theory of heat distribution during welding and cutting. *Welding Journal* 20: 220-s to 234-s.

2. Comini, G., Del Guidice, S., Lewis, R. W., and Zienkiewicz, O. C. 1974. Finite element solution of nonlinear heat conduction problems with special reference to phase change. *Int. J. Num. Meth. Eng.* 8: 613–624.

3. Morgan, K., Lewis, R. W., and Zienkiewicz, O. C. 1978. An improved algorithm for heat conduction problems with phase change. *Int. J. Num. Meth. Eng.* 12: 1191–1195.

4. Pavelic, V., Tanabakuchi, R., Uyehara, O. A., and Myers, P. S. 1969. Experimental and computed temperature histories in gas tungsten arc welding of thin plates. *Welding Journal* 48: 295-s to 305-s.

5. Paley, Z., and Hibbert, P. D. 1975. Computations of temperatures in actual weld design. *Welding Journal* 54: 385-s to 392-s.

6. Goldak, J., Chakravarti, A., and Bibby, M. 1984. A new finite element model for welding heat sources. *Met. Transactions B*, 15B, pp. 299–305.

7. Goldak, J. 1989. Keynote address: Modeling thermal stresses and distortions in welds. Recent trends in welding sciences and technology. *Proc. 2nd Int. Conf. on Trends in Welding Research*, S. A. David and J. M. Vitek, eds. pp. 71–82.

8. Argyris, J. H., Szimmat, J., and William, K. J. 1985. Finite element analysis of arc welding process. *Numerical Methods in Heat Transfer*, Vol III, R. W. Lewis and K. Morgan, eds, Wiley.

9. Kannatey-Asibu, E., Jr., Kikuchi, N., and Jallad, A-R. 1989. Experimental finite element analysis of temperature distribution during arc welding. Trans ASME *J of Mat. & Tech.*, 111: 9–18.

10. Joe, B., and Simpson, R. B. 1986. Triangular meshes for regions of complicated shape. *Int. J. Num. Meth. Eng.*, 23: 751–778.

11. Watson, D. F. 1981. Computing the n-dimensional Delaunay tessellation with application to voronoi polytopes. *Comp. J.* 24: 167–172.

12. Lewis, R.W., Huang, H. G., Usmani, A. S., and Cross, J. T. 1991. Finite element analysis of heat transfer and flow problems using adaptive remeshing including applications to solidification problems. *Int. J. Num. Meth. Eng.* 32: 767–781.